The final decision follows a majority voting mechanism. If at least two models classify the input as anemic, the system labels it as anemic; otherwise, it is classified as non-anemic. By integrating individual predictions, majority voting, and confidence aggregation, the system enhances robustness and interpret-ability, ensuring reliable anemia detection for practical applications.

A. Dataset Collection

The dataset, sourced from the open access web resource \cite{b16} gathered from multiple hospitals in Ghana, consists of images captured by laboratory personnel. The medical officers documented Hb values, age, sex, and anemia status. Dataset consists of 3,392 fingernail images, including 1,696 from anemic individuals and 1,696 from non anemic individuals. The images were captured using high-resolution 12MP cameras with spotlights turned off to minimize ambient light interference. The Region of Interest (ROI) was identified using the threshold triangle method to distinguish the fingernail from the background clearly. In addition, the images were carefully processed to remove shine effects that could affect classification accuracy \cite{b14}. Similar to how fingernail analysis works, the area of interest in the palm dataset was defined using a method called the threshold triangle to improve accuracy in classification. The palm dataset originally had 3,396 images, with 1,698 labeled as anemic and 1,698 as non-anemic. Medical staff adjusted the hand position to ensure high-quality images were taken. This helped eliminate the effect of external lighting, improving the dataset's quality and making it more reliable for training machine learning models. The difference in palm color made it easier to classify anemia based on hemoglobin (Hb) levels \cite{b15}. For the conjunctiva-based anemia detection, a dataset was created using electronic tablets, following a clear protocol for consistency. This dataset had 800 images of the conjunctiva, with 400 showing non-anemic cases and 400 showing anemic cases. The images were processed using a combination of the triangle threshold method and the entropy gray scale image algorithm to effectively extract the region of interest (ROI). This method ensured an accurate depiction of the conjunctiva and reduced the effects of lighting changes on detection models. The dataset also included important information like Hb levels, gender, and age, allowing for detailed analysis. This dataset supports advanced machine learning methods for non-invasive anemia detection using image processing techniques.

B. Model Parameters

Table 1 : Parameters used in Model

Layer (Type)	Output Shape	Param #
ResNet50 (Functional)	(None, 8, 8, 2048)	23,587,712
Global Average Pooling	(None, 2048)	0
Dense	(None, 256)	524,544
Batch Normalization	(None, 256)	1,024
Dropout	(None, 256)	0
Dense	(None, 128)	32,896
Batch Normalization	(None, 128)	512
Dropout	(None, 128)	0
Dense	(None, 64)	8,256
Batch Normalization	(None, 64)	256
Dropout	(None, 64)	0

Dense	**(None, 2)**	**130**

The above table summarizes the architecture and parameters of the Nail, Palm, and Eye models, designed to classify images as anemic or non-anemic. These models use ResNet50, pre-trained on the ImageNet dataset, as the backbone for feature extraction. ResNet50 generates a high-dimensional feature map of shape (None, 8, 8, 2048) and has 23.6 million trainable parameters. A Global Average Pooling (GAP) layer reduces the spatial dimensions by averaging the feature maps, converting them into a single 2048-dimensional feature vector without introducing additional parameters. The network consists of a series of dense layers that progressively reduce the feature dimensions, the first dense layer reduces the feature vector to 256 dimensions with 524,544 parameters, followed by a second dense layer reducing it to 128 dimensions with 32,896 parameters, and a third dense layer reducing it further to 64 dimensions with 8,256 parameters. The final dense layer, with a softmax activation function, outputs two values representing the probability of each class (Anemic or Non-Anemic) and has only 130 parameters. Batch Normalization layers are applied to stabilize training and accelerate convergence, with a small number of parameters in each layer (512 for the 128th layer and 256 for the 64th layer). Dropout layers are used to randomly disable neurons during training, reducing overfitting without increasing the number of parameters.

B. Unified Workflow for Anemia Detection System Using Nail, Palm, and Eye Models

The anemia detection system combines three dedicated deep learning models—NailResNet, PalmResNet, and EyeResNet—each designed to classify images of nails, palms, and eyes, respectively, as either anemic or non-anemic. Below is an integrated overview of the system. The training process for all three models involves:

- Dataset Preparation: Images are labeled as Anemic or Non-Anemic based on hemoglobin (Hb) levels.
- Loss Function: Binary cross-entropy is used to measure classification error.
- Optimizer: The Adam optimizer is employed to minimize the loss function and update model weights.
- Data Augmentation: Techniques such as flipping, rota- tion, and brightness adjustments are applied to improve generalization.
- Evaluation Metrics: Metrics like accuracy, precision, re- call, and F1-score monitor model performance.
- Training Hyperparameters:
  - Epochs: 30.
  - Batch Size: 32.
- Early Stopping and Checkpoints: Prevent overfitting and save the best-performing model.

The flowchart in Fig. 2 illustrates the workflow of an anemia detection system using deep learning models for analyzing images of nails, palms, and eyes. The process begins with users capturing or uploading images, which are then subjected to region of interest (ROI) differentiation through image cropping to focus on relevant features. Further, the images undergo preprocessing, where they are resized to 256×256 pixels and normalized to a range of 0-1 for consistency. Following preprocessing, feature extraction is performed using a ResNet50. These extracted features are then passed through fully connected layers incorporating ReLU activation, batch normalization, and dropout to enhance model learning and prevent overfitting. The system separately classifies images based on different criteria for nails, palms, and eyes. The nail model analyzes nail color and texture to determine anemia status. The palm model assesses palm color and visibility of lines to classify anemia. The eye model examines conjunctival pallor and visible blood vessels in the lower eyelid to predict the anemia. Finally, each model outputs a classification of anemic or non-anemic based on the extracted features and learned patterns enabling a multi-modal approach to anemia detection.

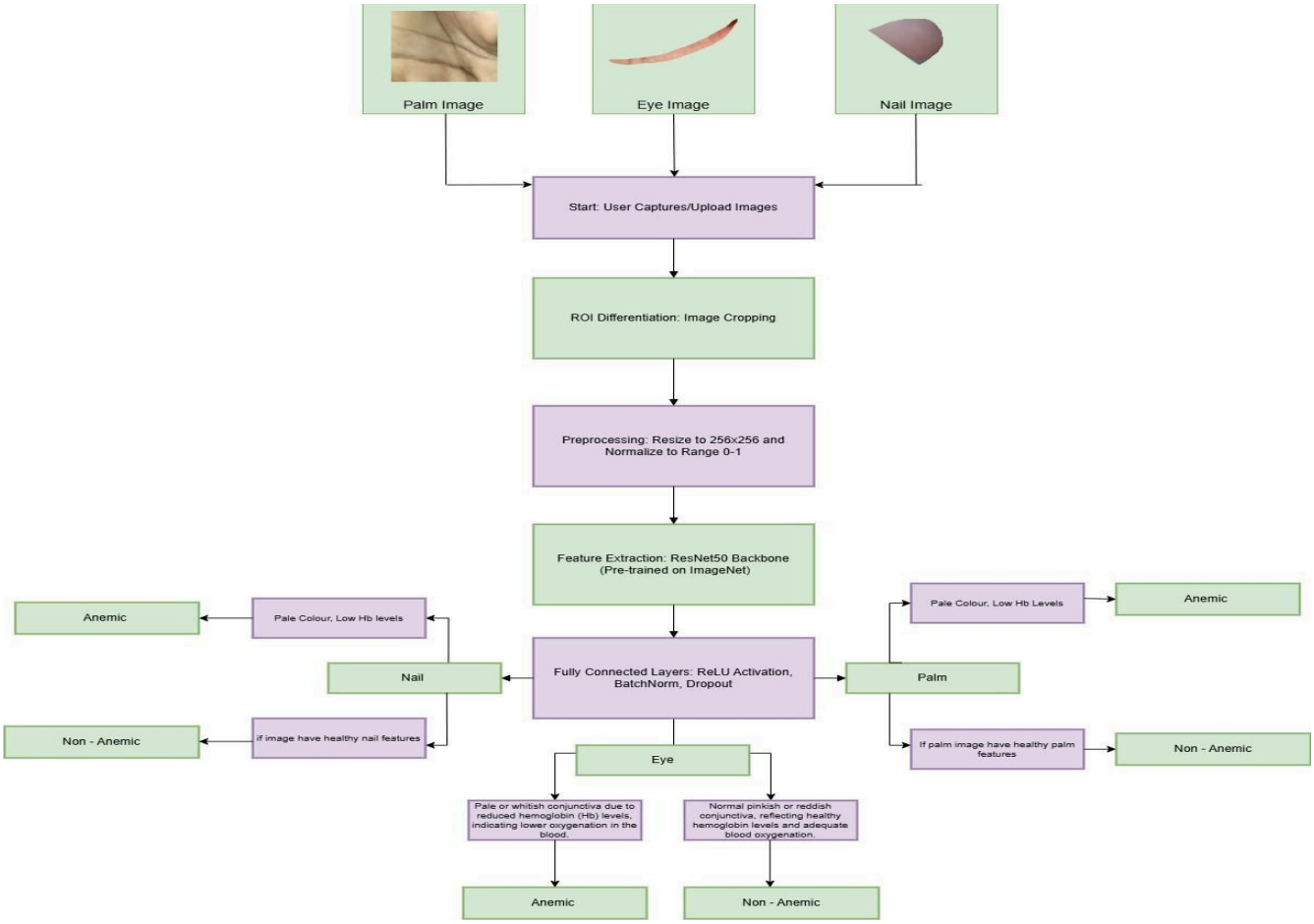

Fig 2 : Workflow for Anemia Detection Using Nail, Palm, and Eye Images

The Algorithm 1, which outlines the anemia classification process using a deep learning-based approach. The method begins by extracting the region of interest (ROI) from the input image, resizing it to a standardized 256 × 256 pixels, and applying normalization to ensure consistent pixel value distribution. Feature extraction is then performed using ResNet50, a state-of-the-art convolutional neural network (CNN), which transforms the normalized image into a high-dimensional feature representation. To refine these extracted features, the algorithm applies a fully connected layer pipeline, incorporating ReLU activation to introduce non-linearity, batch normalization to stabilize learning, and dropout regularization to prevent overfitting. The classification decision follows a set of predefined rules, where the system examines nail, palm, and conjunctiva images for paleness, a key indicator of anemia. If any of these regions appear pale, the input sample is considered anemic. For conjunctiva analysis, hemoglobin (Hb) levels are further evaluated—low Hb confirms anemia, while normal Hb suggests a non-anemic condition. The final classification is determined through a majority voting mechanism, integrating predictions from all three modalities. If at least one of the modalities indicates anemia, the system classifies the input sample as anemic; otherwise, it is labeled non-anemic. This hybrid approach, combining deep learning-based feature extraction with rule-based classification, enhances both the robustness and interpret-ability of the system, making it well-suited for practical anemia detection applications.

Algorithm 1

1) Extract ROI from input image I.

2) Resize I to 256 × 256.

3) Normalize I:

$$I' = I - Imin/Imax - Imin \quad (6)$$

4) Extract feature map F using ResNet50:

$$F = ResN\ et50(I') \quad (7)$$

5) Apply fully connected layers:

a) Frelu ← ReLU (F)

b) Fbn ← BatchN orm(Frelu)

c) Fdrop ← Dropout(Fbn)

6) Decision Rules:

a) If nail is pale ⇒ Anemic, else Non-Anemic.

b) If palm is pale ⇒ Anemic, else Non-Anemic.

c) If conjunctiva is pale:

i) Hblow ⇒ Anemic.

ii) Hbnormal ⇒ Non-Anemic.

7) Final Classification:

C = Anemic, if any modality is Anemic

Non − Anemic, otherwise (8)

IV. RESULTS AND DISCUSSION

)

This section reviews the results of the PalmResNet, NailResNet, and EyeResNet models, highlighting their performance measures in distinguishing between Anemic and Non-Anemic images.

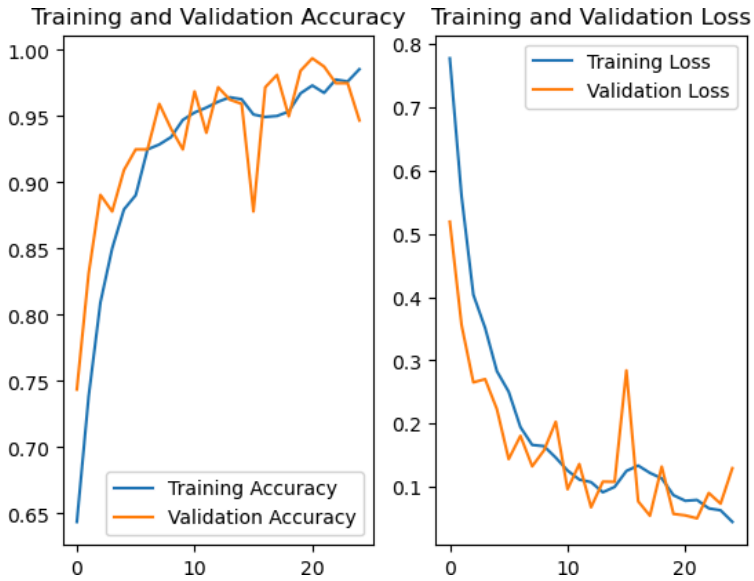

Fig 3 : Training and Validation Accuracy and Loss for PalmResNet Model.

The PalmResNet model demonstrated outstanding performance in classifying palm images. During training, the model achieved an accuracy of 98.64\% with a corresponding loss of 0.0488. For validation, it obtained an accuracy of 94.69\% and a validation loss of 0.1293, reflecting strong generalization capabilities and minimal overfitting. The PalmResNet model effectively leverages ROI differentiation techniques to focus on critical features in palm images. The convergence of the training and validation curves reflects a stable and well-optimized model suitable for real-world anemia detection.

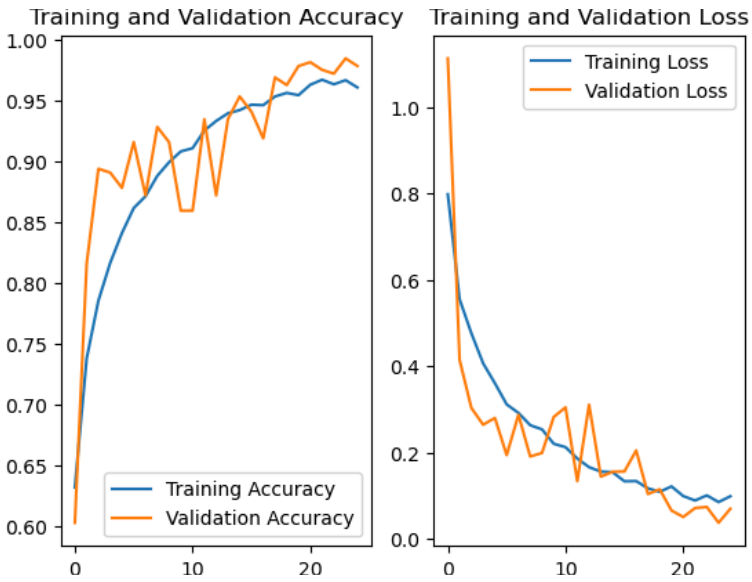

Fig 4 : Training and Validation Accuracy and Loss for NailResNet Model.

The NailResNet model demonstrated good performance in detecting anemia from nail images. It achieved a training accuracy of approximately 96.29 percent and a validation accuracy slightly exceeding 97.81 percent, indicating efficient feature extraction. The accuracy curves suggest a steady improvement over epochs, with validation accuracy consistently tracking training accuracy, signifying a good generalization.The model has a training loss below 0.1 and a validation loss decreasing below 0.1, showing stable convergence. However, the validation loss exhibits some fluctuations, possibly due to variations in the validation data set. While the gap between training and validation loss is minimal, minor overfitting signs can be mitigated with additional regularization techniques.

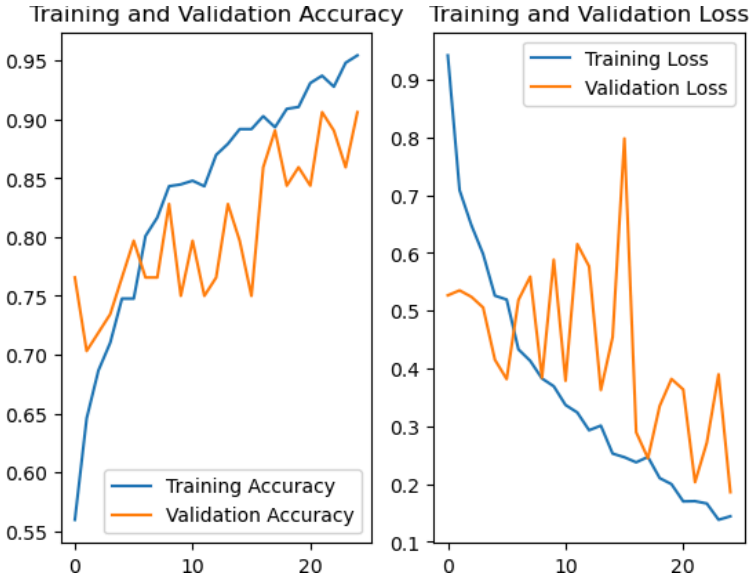

Fig 5 : Training and Validation Accuracy and Loss for EyeResNet Model.

The EyeResNet model demonstrated robust performance in classifying conjunctiva images. In the training phase, the model achieved an accuracy of 95.24\% with a loss of 0.1444. For validation, it achieved an accuracy of 95.62\% and a validation loss of 0.1859, indicating its ability to perform well on unseen data. The EyeResNet model effectively isolates the conjunctiva region using the Threshold Triangle Method, ensuring the focus is on relevant features. Its high accuracy and low loss values ensures its reliability for anemia detection. The below table shows the performance of three distinct deep learning models—LeNet, MobileNet, and ResNet50 across three datasets: Eye, Nail, and Palm. Essential performance measures encompass the number of epochs, training time, accuracy and loss on validation data.

Table 2: Comparison of CNN Algorithms

Dataset	Algorithm	No. of Epochs	Training Time (s)	Validation Accuracy (%)	Validation Loss (%)
Mendeley Eye Dataset	LeNet	25	0.0039	76.19	54.79
	MobileNet	25	4	89.13	32.59
	ResNet50	25	5	95.62	18.59
Mendeley Palm Dataset	LeNet	25	2	84.57	32.72
	MobileNet	25	1.5	91.87	18.32
	ResNet50	25	1	94.69	12.93
Mendeley Nail Dataset	LeNet	25	1	93.75	19.27
	MobileNet	25	1.5	95.26	10.86
	ResNet50	25	2	97.81	6.92

LeNet attains a validation accuracy of 76.19\% and a validation loss of 54.79\%, using 39 milliseconds each epoch. MobileNet achieves 89.13\% accuracy and 32.59\% validation loss, but its training duration extends to 4 seconds per epoch. ResNet50 surpasses both models, with the maximum validation accuracy of 95.62\% and the lowest validation loss of 18.59\%; however, it requires a marginally extended training duration of 5 seconds for each epoch. In the palm dataset, LeNet demonstrates a validation accuracy of 84.57\% and a validation loss of 32.72\%, indicating subpar performance. MobileNet achieves 91.87\% accuracy and 18.32\% validation loss, necessitating merely 1.5 seconds each epoch. Nonetheless, ResNet50 consistently achieves superior performance, attaining a validation accuracy of 94.69\% alongside a reduced validation loss of 12.93\%.In the nail dataset, LeNet attains a validation accuracy of 93.75\% and a validation loss of 19.27\%. MobileNet enhances these metrics to 95.26\% and 10.86\%, respectively. ResNet50 maintains superior performance, achieving 97.81\% accuracy with a validation loss of about 6.92\%.In all datasets, ResNet50 consistently attains the best validation accuracy and the lowest validation loss, rendering it the most efficient model for classifying images of eyes, nails, and palms. Although it requires a marginally extended training duration relative to MobileNet, its enhanced accuracy and reduced loss render it the optimal selection for anemia detection applications.

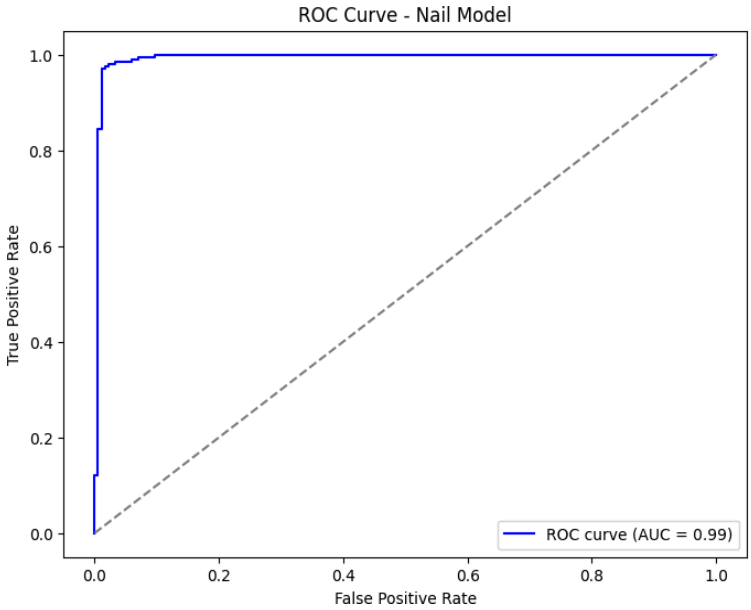

Fig 6 : ROC Curve for Nail Model

The Fig. 6. represents the ROC curve for the nail model. The horizontal axis represents the false positive rate, while the vertical axis indicates the true positive rate. The blue curve illustrates the model's ability to differentiate between positive and negative cases across various threshold values. A curve closer to the top-left indicates better performance. The diagonal dashed line represents a random classifier with equal false positive and true positive rates. The nail model's ROC curve is significantly above this line, indicating strong classification performance. The AUC value of 0.99 suggests that the model performs exceptionally well in distinguishing between classes.

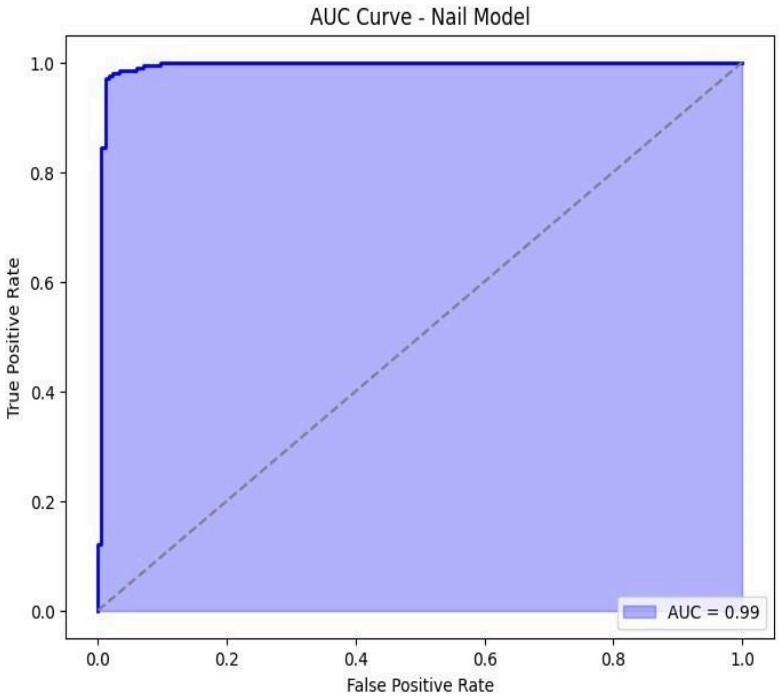

Fig 7 : AUC Curve for Nail Model

The Fig. 7. shows an AUC curve representation of the same model. The area under the ROC curve is shaded in blue, visually emphasizing the high performance of the classifier. The larger the shaded area, the better the model's predictive ability. With an AUC of 0.99, the nail model is nearly perfect in its classification task, meaning it has a very high probability of

correctly ranking a randomly chosen positive instance higher than a randomly chosen negative instance.

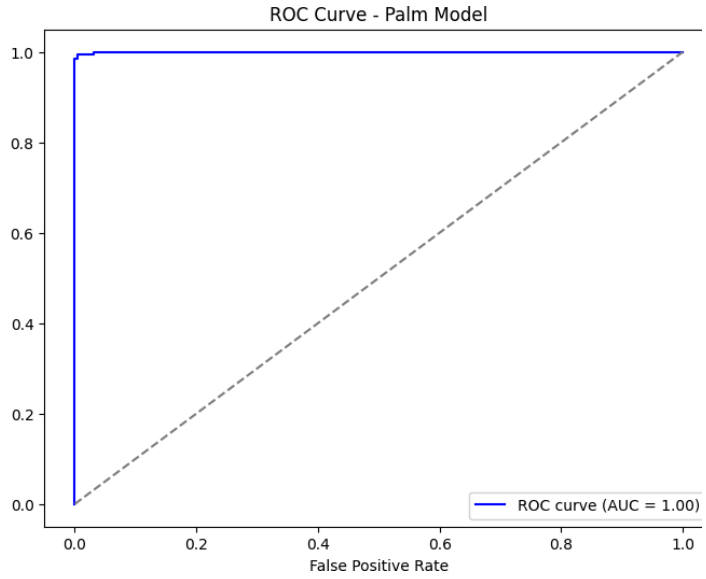

Fig. 8. ROC Curve for Palm Model

The Fig. 8 depicts the ROC curve for the palm model. The x-axis represents the false positive rate, while the y-axis represents the true positive rate. The blue curve illustrates how effectively the model differentiates between positive and negative cases at varying threshold values. The ideal ROC curve is one that reaches the upper-left corner, indicating a perfect classifier. The diagonal dashed line represents a model that makes random guesses, where the false positive rate and true positive rate increase proportionally. The ROC curve for the palm model is almost touching the upper-left corner, showing excellent classification performance. The AUC value of 1.00 signifies that the model has achieved perfect discrimination between classes. The Fig. 9. illustrate second graph displays the AUC curve for the palm model. The shaded blue region highlights the total area under the ROC curve, which quantifies the model's overall performance. Since the AUC value is 1.00, the entire space under the curve is covered, reinforcing that the classifier is performing with perfect accuracy.

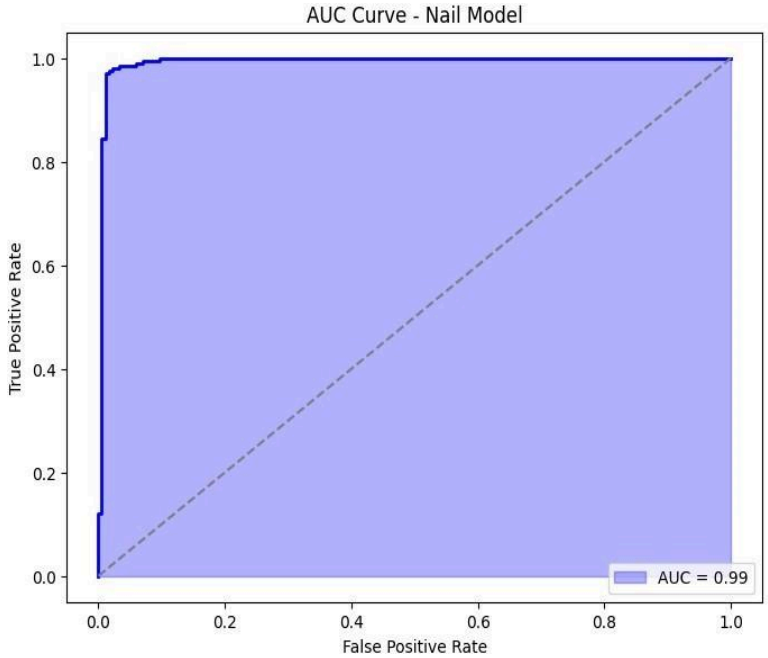

Fig. 9. AUC Curve for Palm Model

A model with an AUC of 1.00 is capable of distinguishing between all positive and negative instances without any misclassification.

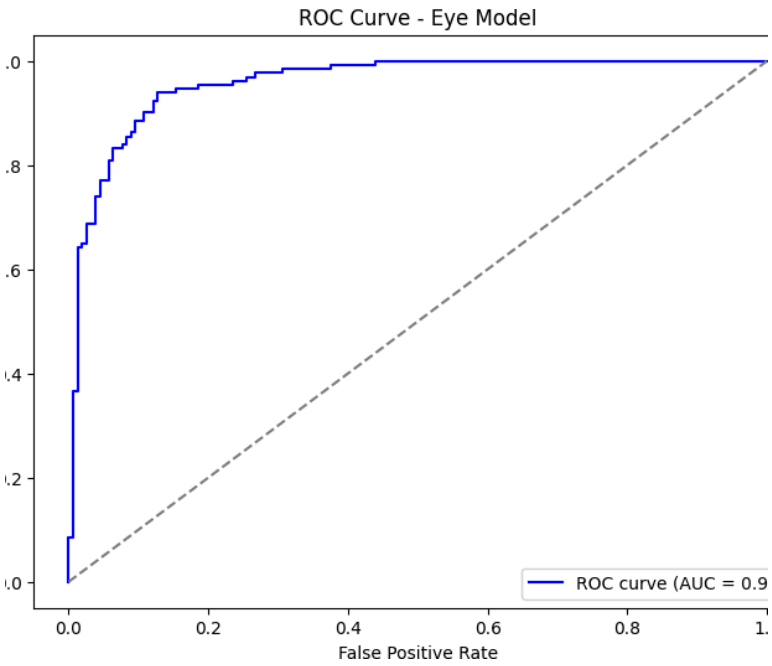

Fig. 10. ROC Curve for Eye Model

The Fig. 10 represents the ROC curve for the eye model. The x-axis represents the false positive rate, while the y-axis represents the true positive rate. The blue curve demonstrates how well the model differentiates between positive and negative cases across different threshold values. A good model has a curve that is close to the upper-left corner, showing high sensitivity with a low false positive rate. The diagonal dashed line represents random classification, where the model would not be better than guessing. The eye model's ROC curve is well above this line, indicating strong classification performance. The AUC value of 0.96 suggests that the model performs very well in distinguishing between different classes, though it is slightly less effective compared to models with an AUC closer to 1.

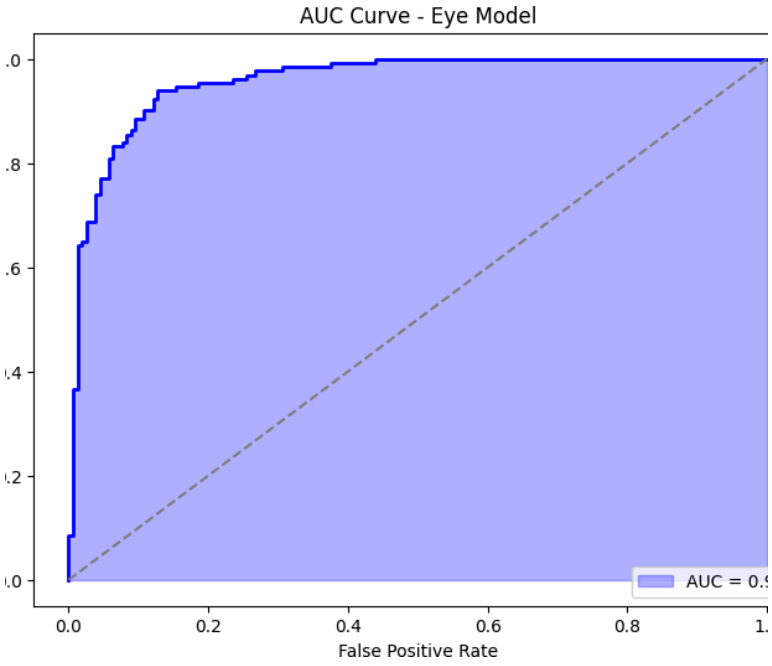

Fig. 11. AUC Curve for Eye Model

The Fig. 11 depicts the AUC curve for the eye model. The shaded blue region highlights the area under the ROC curve, which measures the classifier's overall ability to distinguish between positive and negative samples. Since the AUC value is 0.96, the majority of the space under the curve is filled, reinforcing the fact that the model is highly effective for classification.

A value close to 1 indicates strong predictive ability, though there may still be some misclassification.

V. TEST SAMPLE RESULTS

In order to evaluate the efficiency of the proposed AnemoTech system, test samples from the dataset were selected for analysis based on the three physiological features: nail, palm, and eye conjunctiva. For each test image, it was passed through its corresponding ResNet-based model, namely, NailResNet, PalmResNet, and EyeResNet, respectively. The predicted outputs, with confidence scores, were noted down.

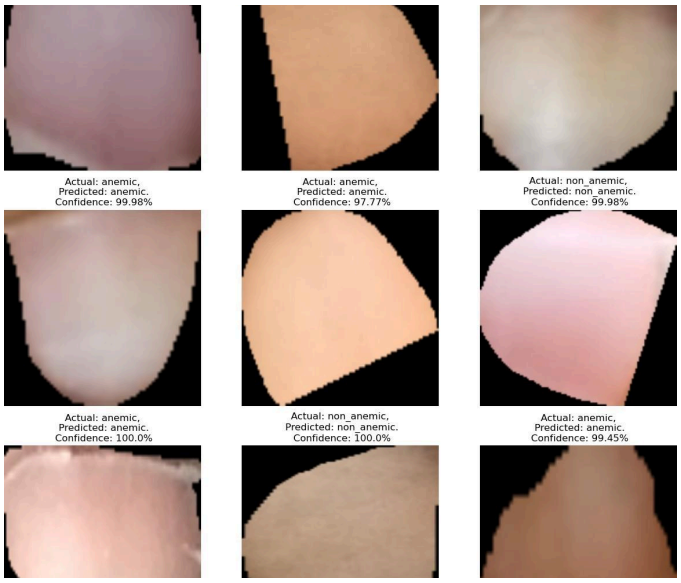

Fig. 12. Nail Image Test Results: Predictions along with confidence scores for test samples classified using NailResNet.

The results for the test samples are illustrated in the images below. Nail image classifications showed excellent distinction between the "Anemic" and "Nonanemic" classes, with confidence at more than 97\% levels for most classifications, except when image quality fluctuations were a problem. The ground truth matched with most predictions in the nail image test, ensuring that NailResNet is doing a good job at extracting features relevant to anemia from the nails.

Fig. 13. Palm Image Test Results: Predictions along with confidence scores for test samples classified using PalmResNet.

The PalmResNet also gave predictions with high confidence. Several samples were predicted to have 99\% or more confidence. The model can differentiate between "Anemic" and "Non-Anemic" samples based on visual cues such as discoloration and texture. In some rare cases, there were lower confidence scores of 57\%, which may have been due to inconsistencies in lighting or palm orientation. Overall, PalmResNet performed well on the identification of anemia from images of palms.

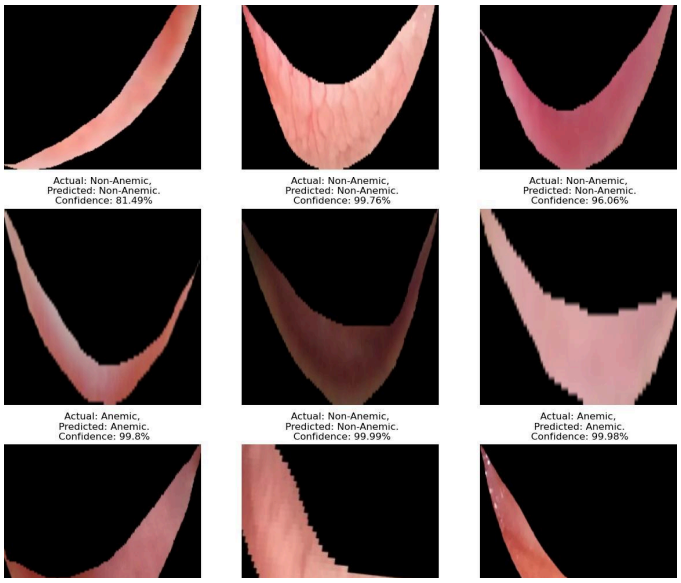

Fig. 14. Eye Conjunctiva Test Results: Predictions along with confidence scores for test samples classified using EyeResNet.

Eye conjunctiva test results showed that EyeResNet classified images with an accuracy of confidence scores above 95\%. In most cases, predictions were perfectly aligned with the ground truth labels, and the model confirmed its ability to analyze paleness in the conjunctiva as an indicator of anemia. Only minimal deviations were observed, which can be attributed to subtle variations in image quality or ROI extraction.

A. Key Observation

The results suggest that the system was reliable for all three physiological features:

1) High confidence scores for most samples indicated model reliability and accuracy.
2) Rare misclassifications or lower confidence scores were likely due to factors such as suboptimal image quality, inconsistent lighting, or improper ROI extraction.
3) Predictions from three different models ensure that the predictions are robust, as the strengths of the models are complementary to each other.

The above results show that this system is poised to be a non-invasive, reliable, and scalable diagnostic method for detecting anemia in several real-world contexts.

VI. CONCLUSION

The proposed work introduced a non-invasive system for detecting anemia using deep learning. The system analyzes images of nails, palms, and eye conjunctiva to overcome the limitations of traditional blood tests, offering a more affordable and accessible alternative. It utilizes ResNet-based models (NailResNet, PalmResNet, and EyeResNet) for precise classification, supported by preprocessing and a majority voting approach. Built with FastAPI, enables real-time predictions, making it suitable for both clinical use and remote healthcare. The proposed system can serve as an assistive technology, aiding medical practitioners in pre-diagnosis by facilitating early detection, improving diagnostic efficiency, and supporting timely decision-making to enhance patient care and treatment outcomes.

Appendix 1 etc. (SIZE 10 & BOLD)

Appendices, if present, must be marked 1, 2, 3, and placed before the below sections.

Interest Conflicts (SIZE 10 & BOLD)

This section is mandatory. When a secondary goal, such as financial gain, influences clinical judgement well about validity of research, a competing interest occurs. In their submitted publications, our authors should declare any potential conflicts of

interest. "The author(s) declare(s) that there is no conflict of interest concerning the publishing of this paper," authors should write if there isn't one. (SIZE 10)

Funding Statement (SIZE 10 & BOLD)
Authors should state how the research and publication of their article was funded, by naming financially supporting bodies followed by any associated grant numbers in square brackets. (SIZE 10)

Acknowledgments (SIZE 10 & BOLD)
The authors would like to sincerely thank family members for their continuous support and patience during the completion of this research. We extend our sincere thanks to MVPS's KBTCOE Nashik for providing the necessary support and computing infrastructure to carry out this research work.

V. REFERENCES (FONT SIZE 10 & BOLD, CAPS)

Experimental Investigation of Tribological Properties of Bio-Based, Nano-Particles

1 Balamurugan M*, 2 Murugapoopathi S,

1*,2 Department of Mechanical Engineering ,PSNA College of Engineering and Technology,Dindigul,Tamilnadu, India, PIN-624622

Abstract:

This study explores the Tribological Properties of bio based, Nanoparticles, at resynthesized by dispersing nanoparticles in nonedible oils, for potential applications in for potential applications in continued lubrication .The Nanoparticles were prepared using Graphene and Jatropha oil through 0.25%, and 0.50% of base oils. Friction and wear tests were conducted using a tribometer against counter face material under various conditions. The Nano particles demonstrated improved lubricity, attributed to the syncretic effects of nanoparticles and vegetable oils. The finding suggest that bio based ,Nano particles as promising eco-friendly alternatives to conventional lubricants, offering enhanced tribological properties and reduced environmental impact.

Keywords: Nanoparticles, Tribology, Environmental, Bio-based oils.

I. INTRODUCTION

Bio-based Nano particles offer a promising alternative to conventional Nano particles due to their biodegradability, non-toxicity, and sustainability. The findings of this study will contribute to the understanding of the tribological behaviour of bio-based Nano particles and their potential applications in lubrication and wear production.

This study explores the use of additives to reduce wear and friction in multilayer Ti-DLC/DLC coatings, focusing on Duraphos® OAP and Duraphos®178 Mobeen Haneef a a, b,*, Liuquan Yang at-el(2024). The results

show sensitivity to changes in operating conditions and can be used for marine thruster seals. Omar Morad *, Raine Viitala, at-el (2024). The study also examines the feasibility of using renewable resources like sunflower, soybean, jatropha oils, and waste cooking oil to produce bio lubricants. Jose M. Limeira Del Rio at-el (2024).The study also investigates the effects of Al2O3 Nano-additives on engine performance and noise emission characteristics in jatropha biodiesel blend.Ali Murtaza Ansari a,Liquat AliMemon a,Mamdouh at-el (2023).The study also investigates the tribological and rheological characteristics of different vegetable oils, with Cuo and Tio2 Nanoparticles improving anti –friction and wear properties C Rajaganapathy a T.V.Rajamurugan at-el (2022).The bio lubricants are characterized using FTIR and TGA analyses, Viscosity, and Viscosity index are evaluated and also their rheological behaviors N.K.Attia⁎,S.A.El-Mekkawi,at-el(2020). However, challenges such as nanoparticle agglomeration and concentration dependence persist. Despite these challenges, bio-based nanoparticles contribute significantly to sustainable engineering practices and help minimize the environmental impact industrial lubricants.

II METHODS

Corresponding authors / EHias'25

3

TRIBOLOGY

VEGETABLE OILS

ULTRASONICATER

COF
BIOLUBRICANTS
PREPARATION PROCESS
PARAMETERSMATERIALS

TESTS

WEAR

Corresponding authors / EHias'25

4

23.52424.52525.52626.52727.52828.5

NANOPARTICLES

2.55
2.6
2.65
2.7
2.75

2.8
2.85
2.9
2.95
3
3.05

Y-Values

Y-Values

Feature Base Oils(Mineral/Synthetic) Bio-based Oils
Source Crude oil(fossil fuel) Renewable resources like
plants,seeds,and algae

Sustainability Non-renewable, potential
environmental impact

Renewable, Biodegradable ,and
environment friendly

Production Refining crude oil Extraction and processing of biomass
Performance Wide range of properties
depending on the base oil type

Often with good biodegradability and low
toxicity

Applications Automotive, industrial
lubricants, greases

Engine oils transmission fluids, and other
applications

Examples Mineral oil, synthetic oil Soybean oil, rapeseed oil, sunflower oil,

castor oil

III.RESULTS AND DISCUSSION

Corresponding authors / EHias'25

5

The study demonstrates that bio-based nanoparticles, including cellulose nanoparticles, chitosan,
and lignin derivatives, exhibit promising tribological properties when compared to conventional synthetic additives.
These nanoparticles significantly reduce the coefficient of friction when dispersed in lubricants, particularly under

high load and sliding velocity conditions. Additionally, they enhance wear resistance, with cellulose Nano crystals facilitating a smoother, more uniform wear surface. While the concentration of bio-based nanoparticles positively correlates with improved tribological performance, excessive concentrations may lead to nanoparticle agglomeration, compromising theireffectiveness.Surface morphology analysis further reveals that bio-based nanoparticle suspensions result in smoother textures and reduced surface damage relative to conventional oils or base lubricants. From an environmental perspective, bio-based nanoparticles offer a substantial advantage over synthetic alternatives due to their biodegradability and lower toxicity.

IV.CONCLUSION

Despite slightly higher production costs, bio-based nanoparticles present long-term cost benefits by minimizing environmental impact and reducing the frequency of lubricant replacement. Moreover, utilized agricultural waste materials for nanoparticle production could further reduce costs, enhancing the economic feasibility of bio-based alternatives. Given their superior sustainability credentials, bio based nanoparticles hold significant promise for industries prioritizing environmental stewardship, such as automotive, manufacturing, and biomedical sectors.

Acknowledgments

Experimental investigation of Tribological properties of Bio Based, Nano-Particles

1 Balamurugan M, 2 Murugapoopathi S.

V.REFERENCES

[1] Mobeen Haneef a a,b,*,Liuquan Yang b,Ardian Morina b,Bruno TRINDADE A,** Super lubricity of multilayer titanium doped DLC coatings by using low SAPS organic additives in base oil TribologyInternational201(2025)110186 https://doi.org/10.1016/j.triboint.2024.110186

[2] Omar Morad*,Raine Viitala,Viitala, Vesa Saikko Behavior of marine thruster lip seals under typical operating conditions https://doi.org/10.1016/j.triboint.2024.110195

[3] José M .Limeira˜del Rio a, b*,Carlos M.C.G.Fernandes b.c,David E.P.Goncalves b,Jorge H.O Seabra c Tribological performance of green nanolubrivcants using functionalized CaCo3 nanoparticles https://doi.org/10.1016/j.triboint.2024.110007

[4] Ali Murtaza Ansari a,Liquat AliMemon a, Mamdouh T Ghannam b,*,Mohamed Y E Selim c,* Impact of biodiesel blended fuel with nanoparticles on performance and noise emission in compression ignition engine https://doi.org/10.1016/j.ijft.2023.100390

[5] C Rajaganapathy a, ⇑,T.V.Rajamurugan a,A.Dyson Bruno ,b,S.Murugapoopathi b,M.Armstrong c A Study on tribological behavior of rice bran and karanja oil-based Tio2 Nano bio-fluids https://doi.org/10.1016/j.matpr.2022.02.071

[6] N.K.Attia⁎,S.A.El-Mekkawi,O.A.Elardy,E.A.Abdelkader Chemical and rheological assessment of produced biolubricants from different vegetable oils https://doi.org/10.1016/j.fuel.2020.117578

Corresponding authors / EHias'25